Preprint typeset using LaTeX style emulateapj v. 5/2/11

arXiv:1604.03329v1 [astro-ph.HE] 12 Apr 2016

AN ULTRA-FAST X-RAY DISK WIND IN THE NEUTRON STAR BINARY GX 340+0

J. M. MILLER[1], J. RAYMOND[2], E. CACKETT[3], V. GRINBERG[4], M. NOWAK[4]

ABSTRACT

We present a spectral analysis of a brief *Chandra*/HETG observation of the neutron star low-mass X-ray binary GX 340+0. The high-resolution spectrum reveals evidence of ionized absorption in the Fe K band. The strongest feature, an absorption line at approximately 6.9 keV, is required at the 5σ level of confidence via an F-test. Photoionization modeling with XSTAR grids suggests that the line is the most prominent part of a disk wind with an apparent outflow speed of $v = 0.04c$. This interpretation is preferred at the 4σ level over a scenario in which the line is H-like Fe XXVI at a modest red-shift. The wind may achieve this speed owing to its relatively low ionization, enabling driving by radiation pressure on lines; in this sense, the wind in GX 340+0 may be the stellar-mass equivalent of the flows in broad absorption line quasars (BALQSOs). If the gas has a unity volume filling factor, the mass ouflow rate in the wind is over 10^{-5} $M_{\odot}$ yr^{-1}, and the kinetic power is nearly 10^{39} erg s^{-1} (or, 5–6 times the radiative Eddington limit for a neutron star). However, geometrical considerations – including a small volume filling factor and low covering factor – likely greatly reduce these values.

Subject headings: accretion disks – X-rays: binaries

1. INTRODUCTION

Accretion onto neutron stars with low magnetic fields is expected to be similar to accretion onto black holes, or at least black holes with low spin parameters. Time scales and line shifts should simply scale with mass, and with the depth of the inner edge of the disk within the potential well. Observations appear to confirm this expectation: quasi-periodic oscillations scale in the expected manner (e.g., Wijnands & van der Klis 1999), and relativistic lines from neutron stars place interesting limits on stellar radii but are not as extreme as lines from spinning black holes (e.g. Cackett et al. 2008, 2010; Di Salvo et al. 2009; Papitto et al. 2009; Miller et al. 2013).

Accretion flows onto neutron stars and black holes might be even more similar, far from the compact object. X-ray disk winds from stellar-mass black holes are emerging as important facets of the accretion flow; in some cases, the mass loss rate can rival or exceed the accertion rate in the inner disk (e.g. King et al. 2012, 2015; Miller et al. 2015). Such winds appear to arise between 10^{2-4} GM/c^2 from the black hole, depending on particulars. Ionized X-ray absorption is commonly observed in neutron star binaries, but evidence of outflowing gas has lagged the rapid progress being made in stellar-mass black holes. Nevertheless, evidence of disk winds in neutron star X-ray binaries is growing, with flows in GX 13+1 (e.g., Ueda et al. 2004) and IGR J17480−2446 (Miller et al. 2011) marking two prominent examples.

In some moderate-resolution spectra of active galactic nuclei (AGN) extremely fast outflows with very high mass fluxes have been observed (e.g., Tombesi et al. 2010). These winds may contribute significantly to feedback and the co-evolution of massive black holes and host galaxies. In stellar-mass black holes, outflow speeds of 0.01–0.05c are detected at gratings resolution (e.g., King et al. 2012, 2015, Miller et al. 2015). Such flows have not previously been reported in the steady emission of neutron star X-ray binaries (but see Pinto et al. 2014 for evidence of fast outflows during bursts).

GX 340+0 is a neutron star X-ray binary, located close to the Galactic Plane. It is known to be a low-mass X-ray binary and a "Z" source based on its behavior in X-ray color-color diagrams (Hasinger & van der Klis 1999). Cackett et al. (2010) analyzed an *XMM-Newton* observation of GX 340+0, and found evidence of a relativistic iron line from the inner disk, strongly impacted by X-ray absorption consistent with H-like Fe XXVI (also see D'Ai et al. 2009). Lavagetto et al. (2004) also found X-ray absorption in a *BeppoSAX* spectrum of GX 340+0; this was modeled with a Gaussian at 6.8 keV. This energy lies between Fe XXV (6.70 keV) and Fe XXVI (6.97 keV), and would imply a large velocity shift. In order to better understand the nature of the ionized X-ray absorption in GX 340+0 at high resolution, we have analyzed archival *Chandra*/HETG spectra of the source.

2. OBSERVATIONS AND REDUCTION

Chandra has observed GX 340+0 on four occasions, but only spectra from ObsID 1922 show evidence of a disk wind; it is the sole focus of this paper. Observation 1922 started on 2001-08-09 at 12:35:11 (UT). After our reduction, we find that a net exposure time of 5.8 ks was achieved.

The data were reduced using CIAO version 4.7 and the associated calibration files. We downloaded the full observation from the *Chandra* archive. The standard sequence of routines, *tgdetect*, *tg_create_mask*, *tg_resolve_events*, and *tgextract* were run to produce first-order spectral files. When executing *tg_create_mask*, we set the parameter "width_factor_hetg" to have a value of 17, rather than the default of 35. This reduces the width of the HEG extraction regions, with the effect of better selecting true first-order HEG photons and enabling the extraction of spectra that carry out to 10 keV. The tools *mkgrmf* and *fullgarf* tasks were run to create response files. Finally, *add_grating_spectra* was run to combine the first-order spectra and responses, and the FTOOL "grppha" was used to group the co-added first-order HEG spectrum to require at least 10 counts per bin.

[1] Department of Astronomy, University of Michigan, 1085 South University Avenue, Ann Arbor, MI 48109-1104, USA, jonmm@umich.edu

[2] Harvard-Smithsonian Center for Astrophysics, 60 Garden Street, Cambridge, MA 02138, USA

[3] Department of Physics & Astronomy, Wayne State University, 666 W. Hancock St, Detroit, MI 48201, USA

[4] Massachusetts Institute of Technology, Kavli Institute for Astrophysics, Cambridge, MA 02139, USA

3. ANALYSIS AND RESULTS

The spectra were fit using XSPEC version 12.8.2 (Arnaud 1996). The "Churazov" weighting scheme was applied in minimizing the χ^2 fitting statistic. All errors reported in this work reflect parameter values at the 1σ confidence limits.

Cackett et al. (2010) report an interstellar column density of $N_{\rm H,ISM} = 0.9 - 1.1 \times 10^{23}$ cm^{-2} along the line of sight to GX 340+0. D'Ai et al. (2009) report similarly high values. This greatly diminishes the low energy flux from this source. Owing to the lack of sensitivity at low energy, and also owing to chip gaps creating calibration uncertainties in the 3–4 keV range, our analysis was restricted to the combined HEG spectrum and the 4–10 keV band.

An initial fit to the spectrum with an absorbed disk blackbody model (*tbabs* × *diskbb*; Wilms et al. 2000, Mitsuda et al. 1984) captures the continuum fairly well, but leaves strong residuals in the Fe K band. The resultant fit statistic is $\chi^2/\nu = 686.37/566 = 1.213$. The implied column density is $N_{\rm H} = 1.5 \times 10^{23}$ cm^{-2}, and the disk temperture is $kT = 0.85$ keV.

Figure 1 depicts this simple model for the spectrum, as well as the data/model ratio, and deviations from the continuum as measured in units of $\Delta\chi^2$. There is a broad flux excess above the continuum in the 5.5–6.5 keV range; this is likely an Fe K emission blurred by effects in the inner accretion disk. D'Ai et al. (2009) and Cackett et al. (2010) both detected this disk line in independent analyses. The most striking and significant feature, however, is an apparent absorption line at 6.9 keV. The addition of a Gaussian model for this line improves the overall fit to $\chi^2/\nu = 641.32/563 = 1.139$.

We performed 2000 Monte Carlo simulations of an absorbed disk spectrum with no line features. We fitted and conducted error bar searches on the resulting spectra with a model including a Gaussian line (emission or absorption) *anywhere* in the 4–10 keV range. The detection of a line feature with equal or greater strength is 99.6% unlikely. This represents a conservative probability for a blind search; in contrast, our search focused on the Fe K band. The change in $\Delta\chi^2$ indicates a line significant at the 5.6σ level of confidence, as measured by an F-test. Counting the number of resolution elements in the 6.7–7.3 keV band as independent trials, the significance is reduced to 5.1σ.

The best-fit line energy is 6.94 ± 0.02 keV. The rest-frame energy of the He-like Fe XXV resonance line is 6.700 keV, and the rest-frame energy of the H-like Fe XXVI resonance line is 6.970 keV (Verner et al. 1996). Thus, the line could represent absorption in a modest inflow, or in a strong outflow. There are weaker features in the 6.5–6.8 keV range and in the 7.0–7.5 keV range that may aid a self-consistent determination of whether the gas is an inflow or outflow.

To address this question, physical self-consistency is required; line-by-line fitting is not sufficient. We therefore constructed a grid of XSTAR photoionized absorption models (e.g., Kallman & Bautista 2001). A turbulent velocity of 300 km s^{-1} and solar abundances were assumed. A nominal gas density of $n = 10^{14}$ cm^{-3} was also assumed. A covering factor must also be specified; we selected $\Omega/4\pi = 0.5$ based on examples of similar absorption in stellar-mass black holes (e.g., Miller et al. 2015). Based on the disk blackbody fit, an input spectrum with $kT = 0.9$ keV and a 2–30 keV luminosity of $L = 4.6 \times 10^{37}$ erg s^{-1} was assumed (based on the unabsorbed flux and an assumed distance of 8.5 kpc; see Penninx et al. 1993) . A grid of models spanning a broad range in column density and ionization was generated using the "xstar2xspec", and included in our subsequent XSPEC fits as a multiplicative table model.

When the grid is allowed to act on the blackbody continuum, it is a 5σ improvement over a model without the absorption, giving $\chi^2/\nu = 648.7/563 = 1.152$. In this fit, $N_{\rm H,wind} = 3.3(7) \times 10^{22}$ cm^{-2} and $\log(\xi) = 3.1(1)$. Importantly, a blue-shift of $v = -0.0395(5)c$ is measured. A model wherein the flow is required to have either zero shift or a red-shift, is significantly worse: $\chi^2/\nu = 671.86/563 = 1.193$. This is true despite the fact that the ionization parameter moves up to $\log(\xi) = 5$, as expected if Fe XXVI must be very strong relative to Fe XXV. An F-test prefers the blue-shifted model over the zero-shift model at the 4.5σ level of confidence. This result does not depend on the interstellar column density; the same blue-shift results when a value of $N_{\rm H,ISM} = 4 \times 10^{22}$ cm^{-2} is enforced (though the overall fit is not as good).

This indicates that the absorption is best associated with an rapid outflow. However, it is possible that the overall spectral model is still too simple. Prior work has found evidence of a relativistic disk line in GX 340+0, and the broad flux excess in Figure 1 appears to confirm this feature in the combined *Chandra*/HEG spectrum. We there added a simple relativistic line, "diskline" (Fabian et al. 1989), in the next model. "Diskline" is characterized in terms of a line energy (restricted to the 6.40–6.97 keV range for Fe I–XXVI in our fits), an disk emissivity index ($J \propto r^q$, bounded to lie in the $-3 \leq q \leq -1$ range), an inner disk radius (measured in units of GM/c^2), an outer disk radius (fixed at 1000 GM/c^2), the inner disk inclination (bounded between $20^\circ \leq \theta \leq 45^\circ$) and a flux normalization.

A model consisting of *tbabs* × *xstar_abs* × (*diskline* + *diskbb*) improves the fit at the 5.6σ level of confidence, to $\chi^2/\nu = 599.1/558 = 1.073$. The absorption is not substantially changed, a blue-shift of $v = -0.0395(6)c$ is again measured ($N_{\rm H,wind} = 2.8 \pm 0.1 \times 10^{22}$ cm^{-2}, $\log\xi = 3.1 \pm 0.1$). The measured diskline parameters include E = $6.4^{+0.1}$ keV, $q = -3^{+0.1}$, $R_{in} = 6.0^{+0.3}$, $\theta = 20^{+1}$, and a normalization of $K = 0.010(1)$ (translating into an equivalent width of $W = 310 \pm 30$ eV). This model is preferred over one including a disline but disallowing blue-shifts at the 4σ level of confidence ($\chi^2/\nu = 618.0/558$).

Weak residuals remain in the Fe K band, suggesting that the wind is more complex than our single-zone model. A model with three zones achieves only modest improvements in the fit statistic, giving $\chi^2/\nu = 590.1/552 = 1.069$. This fit accounts for weaker residuals in the Fe K band, but also fits some apparent lines in the 4–5 keV band that can be associated with He-like Ca XIX and H-like Ca XX (see Figures 2 and 3). We regard this model as our best-fit model; it is fully described in Table 1. The best model wherein all three components cannot be blue-shifted gives $\chi^2/\nu = 637.9/552$ (a 6.6σ difference for a change of one free parameter); the best three-component model wherein only one component is disallowed a blue-shift gives $\chi^2/\nu = 621.4/552$ (a 5.3σ difference for a change of one free parameter).

The data do not require re-emission from the wind; dynamical broadening of such emission can potentially give radius constraints (e.g. Miller et al. 2015, 2016). Winds do not have to be launched with the local escape speed; rather, they can be accelerated continually, or once certain condi-

tions obtain. However, within this framework, an outflow velocity of $v = 0.04c$ corresponds to a launching radius of $r \simeq 1250$ GM/c$^2 \simeq 2.6 \times 10^8$ cm (assuming a neutron star of 1.4 $M_\odot$).

The mass outflow rate in each component can be calculated by starting with the standard formula, $\dot{M} = 4\pi r^2 \rho v$. Adjusting for a non-spherical flow, and writing in terms of number density, the equation becomes $\dot{M} = \Omega \mu m_p n r^2 v$ (where Ω is the covering factor, $\mu = 1.23$ is the mean atomic weight, m_p is the mass of the proton, and n is the number density). Using the ionization parameter (recall, $\xi = L/nr^2$), it is possible to write the mass outflow rate without assuming a density: $\dot{M} = \Omega \mu m_p (L/\xi) v$. The kinetic power in the outflow is then just $L_{kin} = 0.5 \dot{M} v^2$.

For the fast $v = 0.04c$ component detected in GX 340+0, the mass outflow rate is $\dot{M} \simeq 1.1 \times 10^{21}$ g s^{-1}, or $\dot{M} \simeq 1.8 \times 10^{-5}$ $M_\odot$ yr^{-1}. This is a very high mass flux; the implied inflow rate at the inner disk is just 5×10^{17} g s^{-1}, assuming an efficiency of $\eta = 0.1$. The implied power in the fast component is even more extreme: $L_{kin} \simeq 8.1 \times 10^{38}$ erg s^{-1}. This implies that the mechanical power exceeds the radiative eddington limit by a factor of 5–6.

The estimates can be interpreted as the mass outflow rate and kinetic power *divided by the filling factor*. If the volume filling factor is, e.g., $f \simeq 10^{-2}$ (commensurate with some AGN; see, e.g., Blustin et al. 2005), the actual outflow rate is sub-Eddington and the mass outflow rate is also reduced in direct proportion. If the launching radius derived by associating the observed wind speed with a local escape velocity is used, a very high density value results ($n \simeq 1.1 \times 10^{18}$ cm^{-3}), and $f = N_{\rm H,wind}/nr$ implies $f \simeq 1.6 \times 10^{-4}$. This would reduce the mass outflow rate and kinetic power in GX 340+0 by four orders of magnitude. The mass outflow rate would then agree with the inferred mass accretion rate at the inner disk, to within a factor of a few. However, as noted above, there is no requirement that the observed wind speed is a local escape velocity. If the filling factor is not low, it may be the case that GX 340+0 was observed in a super-Eddington phase.

4. DISCUSSION AND CONCLUSIONS

We have analyzed an archival *Chandra*/HETG spectrum of the neutron star low-mass X-ray binary GX 340+0. The spectra reveal strong evidence of a single strong line close to 6.9 keV, and several weaker aborption lines. Self-consistent photoionization modeling establishes that the feature is most likely produced in a complex disk wind, with a component that is blue-shifted by $v = 0.04c$. Even if the wind has a low volume filling factor, its mass outflow rate and kinetic power would still rank among the highest – or as *the* highest – yet detected from a neutron star or stellar-mass black hole. In this section, we discuss the physical processes by which the wind may be driven, and compare the outflow to extreme winds detected in other sources.

Disk winds detected in *Chandra* observations of V404 Cyg and IGR J17091−3634 may offer the best points of comparison for GX 340+0. The 2015 outburst of V404 Cyg was particularly extreme, and it is possible that the mass accretion rate was highly super-Eddington in some phases. In spectra of V404 Cyg, the observed velocity shifts exceed $0.01c$ and the implied mass outflow rate is approximately $\dot{M}_{wind} \simeq 10^{-5}$ $M_\odot$ yr^{-1} (assuming a unity filling factor; King et al. 2015). Spectra of IGR J17091−3624 reveal a wind with two components, with speeds of $0.03c$ and $0.05c$. Here again, the total outflow rate would approach 10^{-5} $M_\odot$ yr^{-1} for a unity filling factor, but the filling factor may be of order 10^{-4} (King et al. 2012).

If the filling factor of the wind in GX 340+0 is not small, the outflow power may actually exceed the observed radiative luminosity. This would likely signal super-Eddington accretion in GX 340+0. The wind would then be driven by electron scattering pressure. At least one ultra-luminous X-ray (ULX) source is powered by a neutron star (Bachetti et al. 2014), and population considerations suggest that a number of ULXs may harbor neutron stars (King & Lasota 2016). However, a super-Eddinton flow is difficult to reconcile with the detection of a relativistic disk line: the central engine should be blocked by a super-Eddington photosphere. Moreover, the observed column density in the outflow is well below $N_{\rm H} \simeq 10^{24}$ cm^{-2} (see Table 1).

Unlike the disk winds that are typically observed in stellar-mass black holes, the wind in GX 340+0 has components with an ionization parameter below $\xi = 10^3$ erg cm s^{-1}. Simulations have identified this as a threshold below which radiation pressure on lines can drive disk winds (e.g., Proga 2003). Directly tapping into the radiative luminosity may help to explain why the outflow in GX 340+0 has a high speed. In this sense, the observed wind may be similar to the extreme outflows in BALQSOs (e.g., Arav et al. 2001).

In BALQSOs, however, geometric shielding is required to keep the gas from becoming over-ionized by X-rays. It is unclear how such shielding might be achieved in an X-ray binary, particularly when the relativistic emission line in this system indicates a clear view of the inner disk (e.g., D'Ai et al. 2009, Cackett et al. 2010). It may be the case that a combination of mechanisms, plausibly including radiative pressure, thermal driving (e.g. Begelman et al. 1983), and magnetic processes (e.g. Blandford & Payne 1982; Proga 2003) act to drive the wind in GX 340+0. It is notable that the inclination angle of $\theta = 35^\circ \pm 1^\circ$ indicated by the relativistic line, is commensurate with the optimal angle for driving magneto-centrifugal winds (Blandford & Payne 1982).

Figure 4 shows the 1.5–12.0 keV *RXTE*/ASM light curve of GX 340+0, spanning intervals near the observation in which we have detected a strong wind, and two subsequent *Chandra* observations that appear to lack strong absorption. The wind is detected in the observation with the lowest flux, though the level is only 10–20% below the observations lacking wind absorption. Hardness ratios might reveal more information, but the ASM ratios are insensitive owing to the very high column density along the line of sight to GX 340+0. Triggered observations based on MAXI light curves and hardness ratios may be able to reveal links between the state of the disk and wind production in GX 340+0.

REFERENCES

Arav, N., et al., 2001, ApJ, 561, 118
Arnaud, K., 1996, Astronomical Data Analysis Software and Systems V, ASP Converence Series, eds. G. H. Jacoby and J. Barnes, 101, 17
Bachetti, M., et al., 2014, Nature, 514, 202
Begelman, M., McKee, C., Shields, G., 1983, ApJ, 271, 70
Blandford, R., & Payne, D., 1982, MNRAS, 199, 883
Blustin, A., Page, M., Fuerst, S., Branduardi-Raymont, G., Ashton, C., 2005, A&A, 431, 111
Cackett, E., Miller J. M., Bhattacharyya, S., Grindlay, J. E., Homan, J., van der Klis, M., Miller, M. C., Strohmayer, T. E., Wijnands, R., 2008, ApJ, 674, 415
Cackett, E., Miller, J. M., Ballantyne, D. R., Barret, D., Bhattacharyya, S., Boutelier, M., Miller, M. C., Strohmayer, T. E., Wijnands, R., 2010, ApJ, 720, 205
Churazov, E., Gilfanov, M., Forman, W., Jones, C., 1996, ApJ, 471, 673
D'Ai, A., Iaria, R., Di Salvo, T., Matt, G., Robba, N., 2009, ApJ, 693, L1
Di Salvo, T., D'Ai, A., Iaria, R., Burderi, L., Dovciak, M., Karas, V., Matt, G., Papitto, A., Piraino, S., Riggio, A., Robba, N., Santangelo, A., 2009, MNRAS, 398, 2022
Fabian, A. C., Rees, M. J., Stella, L., White, N. E., 1989, MNRAS, 238, 729
Hasinger, G., & van der Klis, M., 1989, A&A, 225, 79
Jonker, P., van der Klis, M., Wijnands, R., Homan, J., van Paradijs, J., Mendez, M., Ford, E., Kuulkers, E., Lamb, F., 2000, ApJ, 537, 374
Kallman, T. R., & Bautista, M. A., 2001, ApJS, 133, 221
King, A., & Lasota, J.-P., 2016, MNRAS, arXiv:1601.03738
King, A. L., Miller, J. M., Raymond, J., Fabian, A. C., Reynolds, C. S., Kallman, T. R., Maitra, D., Cackett, E. M., Rupen, M. P., 2012, ApJ, 746, L20
King, A. L., Miller, J. M., Raymond, J., Reynolds, M. T., Morningstar, W., 2015, ApJ, 813, L37
Lavagetto, G., Iaria, R., Di Salvo, T., Burderi, L., Robba, N., Frontera, F., Stella, L., 2004, NuPhS, 132, 616
Miller, J. M., Raymond, J., Fabian, A., Steeghs, D., Homan, J., Reynolds, C., van der Klis, M., Wijnands, R., 2006, Nature, 441, 953
Miller, J. M., Raymond, J., Homan, J., Fabian, A. C., Steeghs, D., Wijnands, R., Rupen, M., Charles, P., van der Klis, M., Lewin, W. H. G., 2006b, ApJ, 646, 394
Miller, J. M., Raymond, J., Reynolds, C. S., Fabian, A. C., Kallman, T. R., Homan, J., 2008, ApJ, 680, 1359
Miller, J. M., Maitra, D., Cackett, E., Bhattacharyya, S., Strohmayer, T., 2011, ApJ, 731, L7
Miller, J. M., et al., 2013, ApJ, 779, L2
Miller, J. M., Fabian, A. C., Kaastra, J. S., Kallman, T., King, A. L., Proga, D., Raymond, J., Reynolds, C. S., 2015, ApJ, 814, 87
Mitsuda, K., Inoue, H., Koyama, K., Makishima, K., Matsuoka, M., Ogawara, Y., Suzuki, K., Tanaka, Y., Shibazaki, N., Hirano, T., 1984, PASJ, 37, 741
Papitto, A., Di Salovo, T., D'Ai, A., Iaria, R., Burderi, L., Riggio, A., Menna, M., Robba, N., 2009, A&A, 493, L39
Penninx, W., Zwarthoed, G. A. A., van Paradijs, J., van der Klis, M., Lewin, W. H. G., Dotani, T., 1993, A&A, 267, 92
Pinto, C., Costantini, E., Fabian, A. C., Kaastra, J., in't Zand, J., 2014, A&A, 563, 115
Ponti, G., Fender, R. P., Begelman, M. C., Dunn, R., Neilsen, J., Coriat, M., 2012, MNRAS, 442, L11
Proga, D., 2003, ApJ, 585, 406
Tombesi, F., Cappi, M., Reeves, J., Palumbo, G., Yaqoob, T., Braito, V., Dadina, M., 2010, A&A, 521, 57
Ueda, Y., Murakami, H., Yamaoka, K., Dotani, T., Ebisawa, K., 2004, ApJ, 609, 325
Verner, D. A., Verner, E. M., Ferland, G. J., 1996, ADNDT, 64, 1
Wijnands, R., & van der Klis, M., 1999, ApJ, 514, 939
Wilms, J., Allen, A., McCray, R., 2000, ApJ, 542, 914

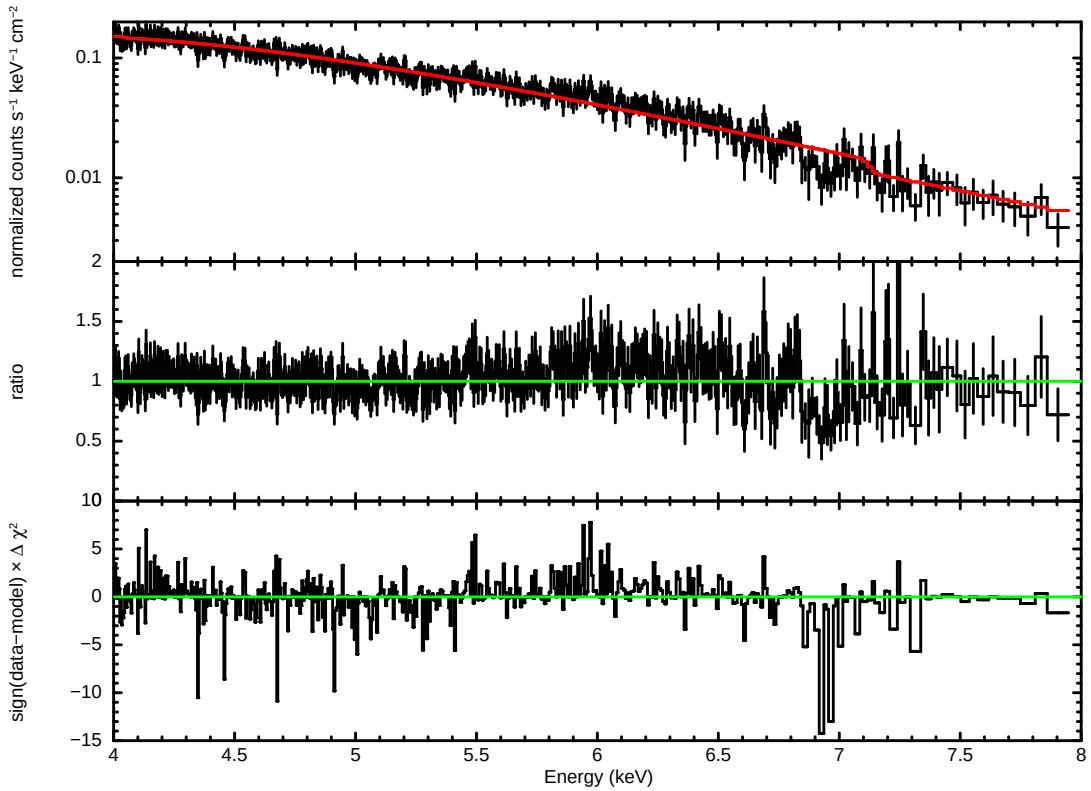

FIG. 1.— The combined first-order HEG spectrum of GX 340+0 from obsid 1922, fit with a simple disk blackbody continuum. The top panel shows the spectrum and model (in red). The middle panel shows the data/model ratio. The bottom panel shows the significance of departures from the continuum, in units of $\Delta\chi^2$. The broad flux excess in the 5.5–6.5 keV range is likely a relativistically blurred Fe K emission line from the inner disk (see, e.g., D'Ai et al. 2009, Cackett et al. 2010). The absorption feature at 6.9 keV could potentially be H-like Fe XXVI (rest frame energy: 6.97 keV) at a modest red-shift, but it is more likely to be is either Fe XXV (rest frame energy: 6.70 keV) at a blue-shift of $\sim$0.04c.

TABLE 1
SPECTRAL FITTING RESULTS

Parameter	Zone 1	Zone 2	Zone 3	Continuum
$N_{H,wind}$ (10^{22} cm^{-2})	4^{+3}_{-1}	8^{+2}_{-1}	$4.7^{+0.8}_{-1.6}$	–
log(ξ)	$4.4^{+0.2}_{-0.6}$	2.38(7)	$2.8^{+0.2}_{-0.1}$	–
v/c (10^{-3})	$-3.6^{+0.7}_{-1.1}$	$-13.3^{+0.7}_{-0.4}$	−39.7(5)	–
$N_{H,ISM}$ (10^{22} cm^{-2})	–	–	–	$10.1^{+1.5}_{-0.3}$
kT (keV)	–	–	–	0.86(1)
diskbb norm.	–	–	–	3000^{+700}_{-300}
$E_{diskline}$ (keV)	–	–	–	$6.40^{+0.03}$
q	–	–	–	$-3.0^{+0.3}$
R_{in} GM/c^2 –	–	–	–	$7.3^{+1.3}_{-0.7}$
θ	–	–	–	35(1)
Norm. (10^{-2}) –	–	–	–	$1.2^{+0.1}_{-0.3}$

NOTE. — The best-fit model to the HEG spectrum of GX 340+0 is detailed above. The overall fit is good, though not formally acceptable: $\chi^2/\nu = 590.07/552 = 1.0690$. Spectral continuum and wind properties are separated for clarity. The continuum was described using a disk blackbody model. A "diskline" component was included to describe a relativistic emission line. The wind was modeled using three XSTAR components, characterized in terms of the wind column density, ionization parameter, and velocity shift ($N_{H,wind}$, ξ, and v/c).

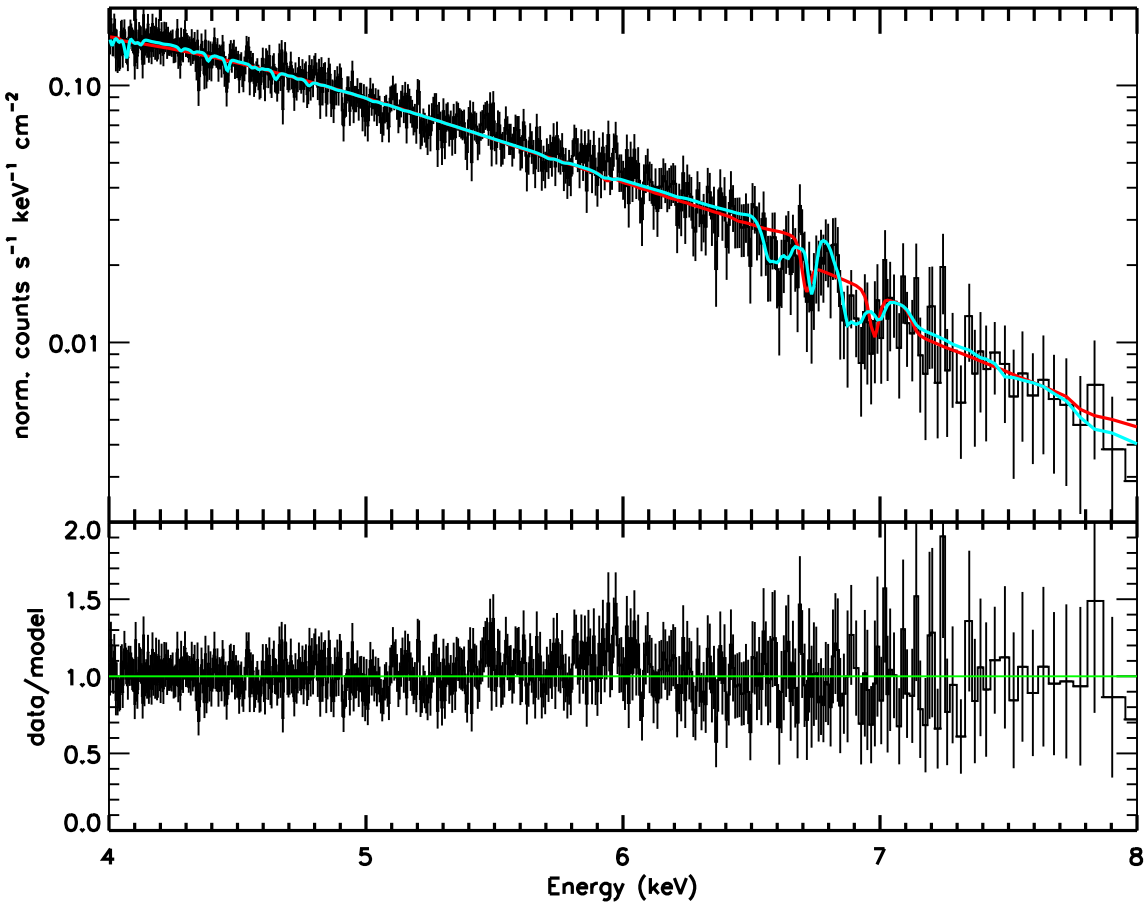

FIG. 2.— The combined first-order HEG spectrum of GX 340+0 from obsid 1922. The best-fit model from Table 1, which includes strong blue-shifts, is shown in cyan. For contrast, the best single-zone model that does not allow blue-shifts is shown in red. The lower panel shows the ratio of the data to the best-fit model.

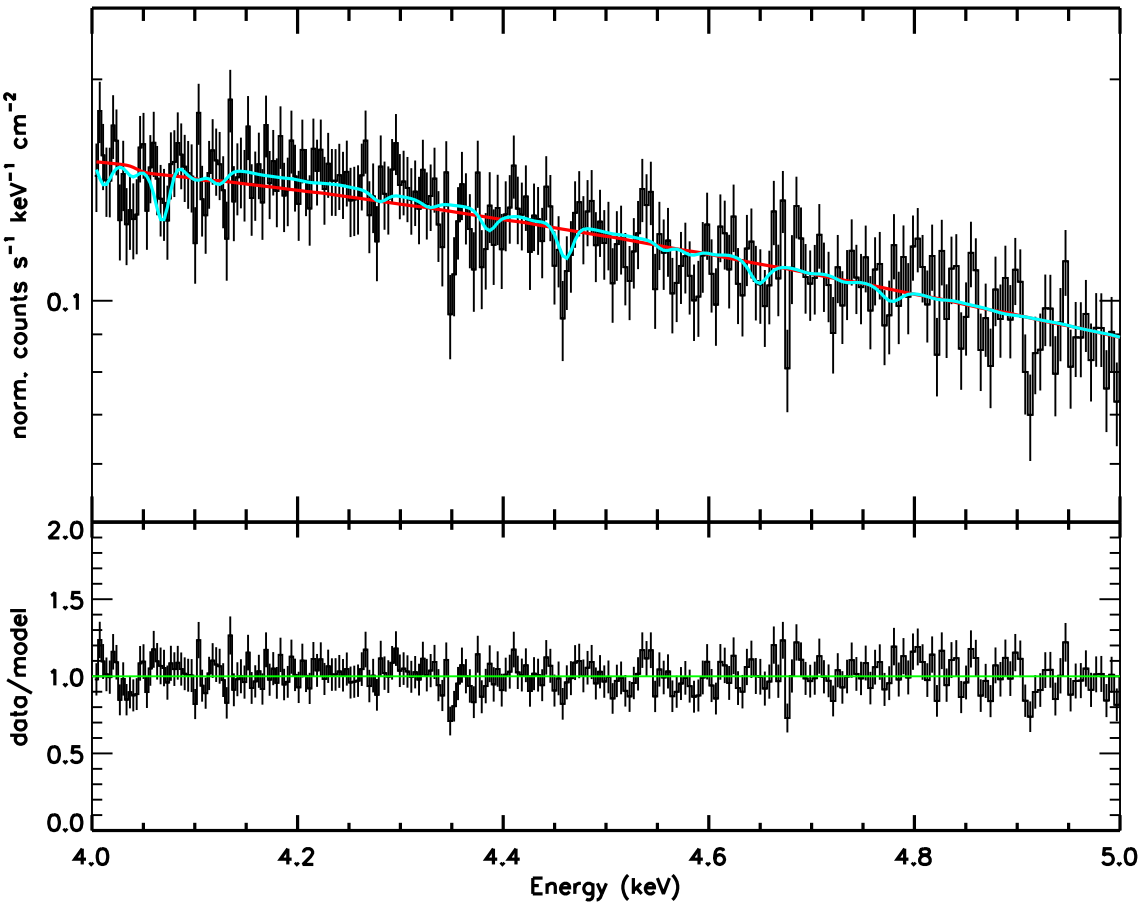

FIG. 3.— The combined first-order HEG spectrum of GX 340+0 from obsid 1922, with the best-fit model shown in cyan (see Table 1). The model is able to explain some of the features in the 4–5 keV range in terms of blue-shifted absorption lines from He-like Ca XIX and H-like Ca XX. For contrast, the model shown in red includes only one absorber, and blue-shifts were disallowed. The lower panel shows the ratio of the data to the best-fit model.

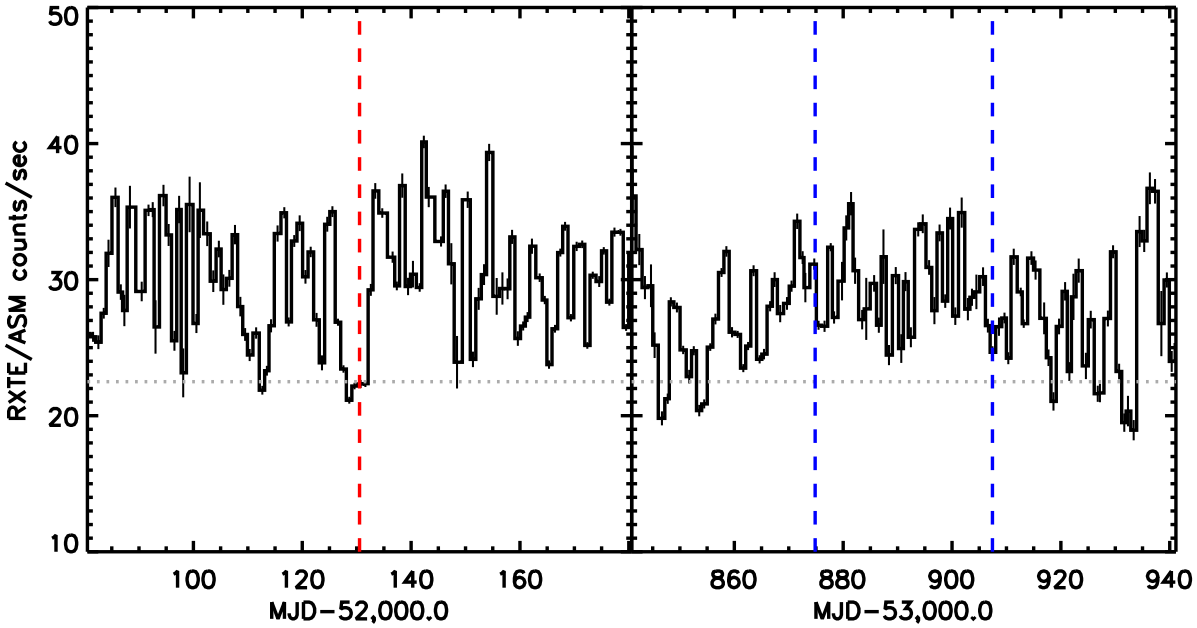

FIG. 4.— Light curves of GX 340+0 from the RXTE/ASM (1.5–12.0 keV). The left panel spans 100 days, centered on *Chandra* ObsID 1922 (dashed red line), in which the relativistic wind is detected. The right panel spans 100 days including ObsIDs 6631 and 6632 (dashed blue lines), in which a wind is not apparent. It is clear that ObsID 1922 was obtained at a lower source flux, and it is possible that such intervals should be targeted in the future to obtain a better understanding of the wind in GX 340+0. Dashed, gray horizontal lines indicate the flux level at which ObsID 1922 was obtained.